Dalton Transactions

PAPER

Cite this: *Dalton Trans.*, 2018, **47**, 5083

Thermodynamic properties of selenoether-functionalized ionic liquids and their use for the synthesis of zinc selenide nanoparticles†

Karsten Klauke,[a] Dzmitry H. Zaitsau,[b] Mark Bülow,[c] Li He,[a] Maximilian Klopotowski,[a] Tim-Oliver Knedel,[a] Juri Barthel,[d] Christoph Held,*[c] Sergey P. Verevkin*[b] and Christoph Janiak*[a]

Three selenoether-functionalized ionic liquids (ILs) of *N*-[(phenylseleno)methylene]pyridinium (**1**), *N*-(methyl)- (**2**) and *N*-(butyl)-*N*′-[(phenylseleno)methylene]imidazolium (**3**) with bis(trifluoromethanesulfonyl)imide anions ([NTf_2]) were prepared from pyridine, *N*-methylimidazole and *N*-butylimidazole with *in situ* obtained phenylselenomethyl chloride, followed by ion exchange to give the desired compounds. The crystal structures of the bromide and tetraphenylborate salts of the above cations (**1-Br**, **2-BPh$_4$** and **3-BPh$_4$**) confirm the formation of the desired cations and indicate a multitude of different supramolecular interactions besides the dominating Coulomb interactions between the cations and anions. The vaporization enthalpies of the synthesized [NTf_2]-containing ILs were determined by means of a quartz-crystal microbalance method (QCM) and their densities were measured with an oscillating U-tube. These thermodynamic data have been used to develop a method for assessment of miscibility of conventional solvents in the selenium-containing ILs by using Hildebrandt solubility parameters, as well as for modeling with the electrolyte perturbed-chain statistical associating fluid theory (ePC-SAFT) method. Furthermore, structure–property relations between selenoether-functionalized and similarly shaped corresponding aryl-substituted imidazolium- and pyridinium-based ILs were analyzed and showed that the contribution of the selenium moiety to the enthalpy of vaporization of an IL is equal to the contribution of a methylene (CH_2) group. An incremental approach to predict vaporization enthalpies of ILs by a group contribution method has been developed. The reaction of these ILs with zinc acetate dihydrate under microwave irradiation led to ZnSe nanoparticles of an average diameter between 4 and 10 nm, depending on the reaction conditions.

Received 18th January 2018,
Accepted 12th March 2018

DOI: 10.1039/c8dt00233a

rsc.li/dalton

Introduction

Ionic liquids (ILs), in particular room temperature ILs such as [BMIm][BF_4], [BMIm][PF_6] or [BMIm][NTf_2], have attracted considerable attention in recent years due to their diverse applications, *e.g.* in the fields of catalysis,[1,2] analytics,[3,4] electrochemistry,[5] CO_2-capturing,[6–8] energy storage and generation[9–11] as well as for material synthesis.[12–15] Accordingly, ILs were used as non-conventional solvents for organic and inorganic reactions with an expectation of unusual results compared to conventional organic solvents.[16–21] In particular, the synthesis of nanomaterials in ILs was possible without the addition of capping ligands so as to retain the surface activity of the nanoparticles.[22] For example, ILs have a low interfacial tension, which in turn leads to a high nucleation rate and thus to smaller particles.[23] In addition, ILs have an intrinsic "nanostructure" caused by hydrogen bonds and electrostatic and van der Waals interactions, which enables both an electrostatic and steric (electrosteric) stabilization of nanoparticles.[22,24,25]

In many cases, ILs are considered inert solvents. However, since 2000 the increasing number of publications dealing with the chemical and thermal stability of ILs has questioned the assumed inertness.[26–36] For example, the thermal stability of

[a]*Institut für Anorganische Chemie und Strukturchemie, Heinrich-Heine-Universität Düsseldorf, Universitätsstraße 1, 40225 Düsseldorf, Germany. E-mail: janiak@uni-duesseldorf.de*
[b]*Department of Physical Chemistry, Universität Rostock, Dr.-Lorenz-Weg 2, 18059 Rostock, Germany. E-mail: sergey.verevkin@uni-rostock.de*
[c]*Technische Universität Dortmund, Emil-Figge-Str. 70, 44227 Dortmund, Germany. E-mail: Christoph.Held@tu-dortmund.de*
[d]*Gemeinschaftslabor für Elektronenmikroskopie RWTH-Aachen, Ernst-Ruska-Centrum für Mikroskopie und Spektroskopie mit Elektronen, Forschungszentrum Jülich GmbH, 52425 Jülich, Germany*

†Electronic supplementary information (ESI) available: IL synthesis and characterization, QCM measurements, nanoparticle synthesis. CCDC 1589574–1589576. For ESI and crystallographic data in CIF or other electronic format see DOI: 10.1039/c8dt00233a

ILs, which is highlighted in most publications, is typically based on thermogravimetric analyses (TGA), which is a dynamic method and provides only a short-term stability of the compound.[31,34] A thermal degradation of an IL can also occur over a longer period of time, such as hours or days at significantly lower temperatures than the TGA might suggest.[34,36–38] In terms of the chemical stability of ILs, it was also shown that a large number of reactions, such as the formation of carbene complexes, reactions with CO_2, CS_2, OCS or chalcogenides, the cleavage of C–N bonds and nucleophilic reactions or the hydrolysis of anions under suitable conditions are possible.[26–30]

A designed reactivity of ILs may even be advantageous. This was demonstrated by the use of ILs as precursor compounds (termed: Ionic Liquid Precursors, ILPs) for the synthesis of nanoparticles. Examples are the synthesis of metal fluoride or metal oxide nanoparticles using ILs such as [BMIm][BF_4],[39,40] [BMIm][PF_6],[41] or tetrabutylammonium hydroxid.[42–44] Mesoporous carbon/iron carbide hybrid nanoparticles were synthesized using mesoporous silica as template and the IL [BMIm][$FeCl_4$] as carbon and iron source.[45] CuCl[46] and Sb_2Se_3 and Bi_2Se_3 [47] nanoplatelets were obtained from the halometalate IL with 6-*O*-palmitoyl ascorbic acid or $(Et_3Si)_2Se$, respectively.

These examples make it apparent that knowledge of the chemical and thermodynamic properties of ILs is an important aspect in terms of their respective application. Trial and error methods for the selection of a suitable IL are of course not practical. It is therefore important to understand the properties of ILs at the molecular level in order to develop theoretical models that accurately predict their properties over a wide temperature and pressure range. These models include structure–property relationships[48–51] and more holistic approaches such as the perturbed-chain statistical associating fluid theory (PC-SAFT) and its various variants.[52–57] In the past, the electrolyte perturbed-chain statistical associating fluid theory (ePC-SAFT) was successfully applied to predict *e.g.* densities and gas solubility[52] for different imidazolium-based ILs and their mixtures with common solvents.[52]

Herein, we synthesized three examples of the selenoether-functionalized ILs containing the [NTf_2]-anion in order to investigate their thermodynamic properties: vapor pressures, vaporization enthalpies and densities. The results have been used to develop parameters of the empirical method (Hildebrand solubility parameters) and the theoretical ePC-SAFT method. Both methods are able to predict the solubility of precursors of ionothermal synthesis reactions, as well as common solvents in the selenium-containing ILs. All three ILs studied were used as ILPs for the synthesis of ZnSe nanoparticles.

Results and discussion

Synthesis of the ionic liquids

The halide salts of of *N*-[(phenylseleno)methylene]pyridinium (**1**), *N*-(methyl)- (**2**) and *N*-(butyl)-*N*'-[(phenylseleno)methylene] imidazolium (**3**) (**1-Br**, **2-Cl** and **3-Br**, respectively) were prepared in a two-step synthesis under inert conditions based on literature procedures of closely related ILs (Scheme 1).[58] The first step involves the *in situ* formation of phenylselenomethylene chloride from diphenyl diselenide, which is used in the second step for the alkylation of pyridine or imidazole. The colorless to yellowish crystalline products were obtained in yields of 50–90% and were characterized *via* ^{1}H-, ^{13}C- and ^{77}Se-NMR-spectroscopy as well as electron spray ionization mass spectrometry (ESI-MS). The ^{1}H-NMR spectra reveal a signal of the methylene group at 5–6 ppm, with small selenium satellites. In the ^{77}Se-NMR spectra a singlet occurs between 440 and 500 ppm. The melting points of the halides (**2-Cl**) and (**3-Br**) lie below 100 °C (Table 1).

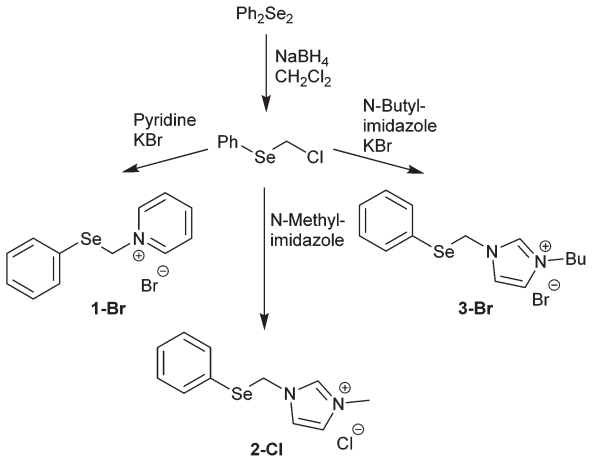

Scheme 1 Synthetic methodology for the preparation of **1-Br**, **2-Cl** and **3-Br**.

Table 1 Overview of the melting points of the synthesized compounds

Compound	Melting point [°C]
1-Br	155.6
2-Cl	98.1
3-Br	66.0
1-NTf_2	<R.T.
2-NTf_2	<R.T.
3-NTf_2	<R.T.
2-BPh_4	164.2
3-BPh_4	110.5

The halide containing ILs are not practical due to their hygroscopic character and high melting points while the corresponding and hydrophobic [NTf_2]-containing salts (**1-** to **3-NTf_2**) are room-temperature ILs (Table 1). The latter were prepared by an aqueous ion exchange reaction with Li[NTf_2] (Scheme 2).

The purity of the [NTf_2]-ILs (**1-** to **3-NTf_2**) was verified by ion-chromatography (IC) yielding an anion purity of all three ILs of over 99% (Fig. S1 and Table S1†).

Although thermogravimetric analysis (TGA) often does not adequately describe the thermal stability of ILs over an

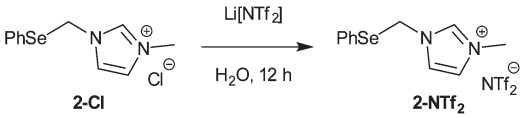

Scheme 2 Synthetic methodology of the aqueous ion-exchange exemplified for the reaction *N*-(methyl)-*N*′-[(phenylseleno)methylene]-imidazolium chloride (**2-Cl**) to the respective [NTf_2]-IL (**2-NTf_2**).

extended time, TGA measurements of the selenoether-functionalized pyridinium salt (**1-Br**) and the ILs **2-Cl**, **3-Br** and **1-** to **3-NTf_2** have been performed as preliminary stability indicators (Fig. S29†). The TGA curves showed a significantly lower decomposition temperature of the halides (180–220 °C) over the [NTf_2]-ILs (225–295 °C).

In order to obtain a crystal structure elucidation of the imidazolium IL-cations **2** and **3**, the room-temperature solid and non-hygroscopic tetraphenylborate salts (**2-BPh_4** and **3-BPh_4**) (Fig. 2 and 3) were prepared by an ion exchange reaction with the Na[BPh_4] in ethanol.

Crystal structure determination

The compounds **1-Br**, **2-BPh_4** and **3-BPh_4** could be grown as colorless to yellowish crystals from $CHCl_3$ or $CHCl_3$/EtOH.

The molecular structure of the *N*-[(phenylseleno)methylene]pyridinium bromide (**1-Br**) (Fig. 1) shows a phenyl ring inclined towards the pyridinium ring. The interplanar angle of 27.0(1)° and a centroid–centroid distance of 4.08(1) Å speak against significant intramolecular π-interaction. Instead, the supramolecular package exhibits intermolecular pyridinium–phenyl interactions with a centroid–centroid distance of 3.73(1) Å and an interplanar angle of 3.7(1)°.[59]

The packing in **1-Br** is organized by Coulomb interactions which are supported by secondary interactions such as, C–H···Br,[60] Se···Se (3.44(1) Å) and Se···Br (3.52(1) Å) contacts (Fig. S30–S33 and Tables S3–S5†). The van der Waals radii of selenium and bromine are 1.90 and 1.85 Å, respectively.

Both compounds **2-BPh_4** and **3-BPh_4** feature crystal structures with a high number of symmetry-independent molecules, resulting in values of $Z' > 1$. Such $Z' > 1$ structures can derive from a metastable structure, that is often referred to as "a crystal on the way" or "frustrated", since such structures often reveal a competition or a balance of several strong and special supramolecular (*e.g.* hydrogen bonding, interhalogen or π–π) interactions between the symmetry-independent units.[61–65]

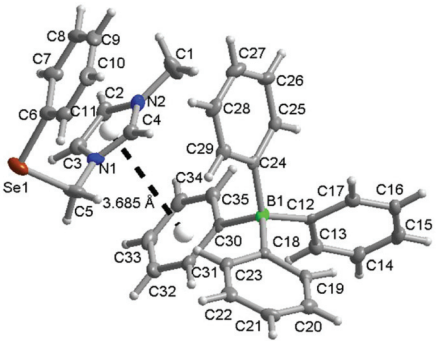

Fig. 2 Molecular structure of *N*-methyl-*N*′-[(phenylseleno)methylene)]imidazolium tetraphenylborate (**2-BPh_4**) with imidazolium-phenyl π-interactions between cation and anion (50% thermal ellipsoids and H-atoms of arbitrary radii). Only one ion pair out of the four symmetry-independent ion pairs in the asymmetric unit is shown for clarity (see Fig. S34† for the full asymmetric unit).

The compound *N*-methyl-*N*′[(phenylseleno)methylene)]imidazolium tetraphenylborate (**2-BPh_4**) crystallizes with an asymmetric unit consisting of four symmetry-independent ion pairs to give $Z' = 4$ (Fig. S34,† only one ion pair shown in Fig. 2). Besides the predominant Coulomb interactions, the molecular packing features C–H···π interactions (Tables S6–S8, Fig. S35–S38†).[66]

The compound *N*-[(phenylseleno)methylene)]-*N*′-butylimidazolium tetraphenylborate (**3-BPh_4**) crystallizes with two symmetry-independent ion pairs in the asymmetric unit, $Z' = 2$. The two cations differ in the C–Se–C–N torsion angle (Fig. 3). With a torsion angle of 60.8(1)° conformer 1 has the phenyl ring oriented towards the imidazolium ring analogously to compound **1-Br** and **2-BPh_4**. In conformer 2 the phenyl ring is facing away from the imidazolium ring (torsion angle: −89.3(2)°). Also in **3-BPh_4** the Coulomb interactions are supplemented by C–H···π interactions (Fig. S40–S43 and Tables S9, S10†).[66]

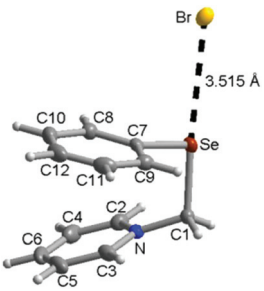

Fig. 1 Molecular structure of *N*-[(phenylseleno)methylene]pyridinium bromide (**1-Br**) with one of the secondary Se···Br interactions (50% thermal ellipsoids, H-atoms of arbitrary radii).

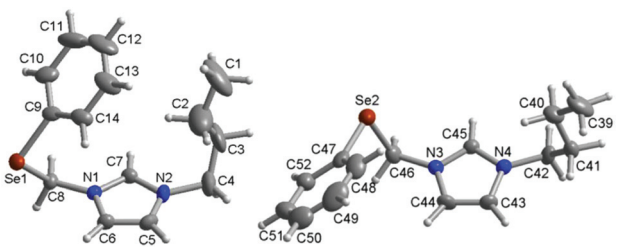

Fig. 3 Molecular structures of both cation conformers in *N*-butyl-*N*′-[(phenylseleno)methylene)]imidazolium tetraphenylborate (**3-BPh_4**) (50% thermal ellipsoids, H-atoms of arbitrary radii, anions have been omitted for clarity, see Fig. S39† for the full asymmetric unit).

Absolute vapor pressures of the selenoether-functionalized ILs with [NTf_2]-anion

Admittedly, ILs have a negligible vapor pressure at ambient temperatures, however the practical applications as catalysts or thermofluids are performed at elevated temperatures and for this reason the knowledge of IL's absolute vapor pressure is required for safety reasons as well as to assess mass uptake during the long-term processing. The frequency changes rates ($df/d\tau$) measured by a quartz-crystal microbalance (QCM) were used for calculation of the absolute vapor pressures p_{sat} of the ILs according to eqn (5) (Table S12†) with help of the empirical constant K' evaluated for our experimental setup recently.[67] The temperatures 373 K and 473 K seem to be a reasonable choice for many practical applications, such as the usage of ILs as extraction agents[68] or as solvents for chemical reactions,[69] and ILs are also important for electric battery applications or usable as entrainers for azeotrope braking. Further, extremely low values of vapor pressures of the ILs **1-** to **3-NTf_2** at these temperatures (Table 2) indicate that the negligible mass uptake of the IL in different catalytic or separation applications can be expected even at elevated temperatures.

It has turned out that irrespective of the structure of the cation the absolute vapor pressures of the selenium-containing ILs are on a comparable level, but they are about three to four times lower in comparison to the structurally parent ILs without selenium (*e.g.* comparison of **3-NTf_2** and [*N*-butyl-*N*′-phenylimidazolium][NTf_2], **4**).

Table 2 Absolute vapor pressures of ILs **1–3-NTf_2**, **4** and **8** at 373 K and at 473 K

IL	$10^{-7} \times p_{sat}$, [Pa] 373 K	$10^{-3} \times p_{sat}$, [Pa] 473 K
1-NTf_2	0.70	2.6
2-NTf_2	25	0.25
3-NTf_2	7.9	5.1
4[a]	26	19
8[b]	17	9.4

[a] See Fig. 4 for the structure of **4**. Vapor pressure measurements published in ref 75 were evaluated using the calibration coefficient developed in our recent work.[67] [b] See Fig. 4 for the structure of **8**. Vapor pressure measurements published in ref. 72 were evaluated using the calibration coefficient developed in our recent work.[67]

Molar vaporization enthalpies from vapor pressure measurements

Vapor pressures and vaporization enthalpies of the selenoether-functionalized ILs have been measured for the first time. The standard molar enthalpies of vaporization derived from the temperature dependence of the vapor pressures measured with the QCM (Table 3, column 4) are referenced to the average temperature T_{av} (Table 3, column 3), which is the middle of the temperature range under study. However, the measured enthalpies of vaporization $\Delta_l^g H_m^\circ(T_{av})$ have to be adjusted to the reference temperature 298.15 K, for the purpose of comparison with results derived from other methods and for the understanding of the structure–property relations. In order to adjust vaporization enthalpies to this temperature the $\Delta_l^g C_{p,m}^\circ$-values are required. Formally, the value $\Delta_l^g C_{p,m}^\circ = C_{p,m}^\circ(g) - C_{p,m}^\circ(l)$ is the difference of the molar heat capacities of the gaseous $C_{p,m}^\circ(g)$ and the liquid phase $C_{p,m}^\circ(l)$, respectively. As a rule, the values of $C_{p,m}^\circ(l)$ are often available in the literature or even they can be assessed by some simple empirical rules.[70] In our recent work,[70] we suggested a simple way for the estimation of the $\Delta_l^g C_{p,m}^\circ$-values, which is based on the experimental data of $C_{p,m}^\circ(l,\ 298.15\ K)$ of the imidazolium-based ILs containing a [NTf_2]-anion and developed the empirical equation (eqn (1)) (in J K^{-1} mol^{-1}):

$$\Delta_l^g C_{p,m}^\circ = C_{p,m}^o(l,\ 298.15\ K)(-0.26 \pm 0.05) + (68.7 \pm 37.0). \quad (1)$$

Taking into account the similar shape of the [C_nMIm][NTf_2] and the selenoether-functionalized containing ILs from this study, we estimated the $\Delta_l^g C_{p,m}^\circ$-values according to eqn (1), using the $C_{p,m}^\circ(l,\ 298.15\ K)$-values assessed in Table 4. In the total absence of physico-chemical data for selenoether-functionalized ILs, the same procedure was also applied for the pyridinium-based ILs containing selenium. The $C_{p,m}^\circ(l,\ 298.15\ K)$ and the $\Delta_l^g C_{p,m}^\circ$-values are required for the temperature adjust-

Table 3 Thermodynamics of vaporization of the selenoether-functionalized ILs derived from QCM measurements

Cation	T-range [K]	T_{av}	$\Delta_l^g H_m^\circ(T_{av})$ [kJ mol^{-1}]	$\Delta_l^g G_m^\circ(T_{av})$[a] [kJ mol^{-1}]	$\Delta_l^g C_{p,m}^\circ$[b] [J K^{-1} mol^{-1}]	$\Delta_l^g H_m^\circ(298.15\ K)$[c] [kJ mol^{-1}]
Column 1	2	3	4	5	6	7
1	378–433	407.3	155.2 ± 3.0	80.4 ± 1.4	−89	164.9 ± 3.6
2	369–406	388.1	123.7 ± 1.0	73.8 ± 1.4	−93	132.1 ± 2.0
3	369–416	391.3	132.2 ± 1.0	76.6 ± 1.3	−118	143.2 ± 2.4
4	363–408	385.0	132.3 ± 1.0	73.7 ± 1.4	−65	137.9 ± 2.0[75]
5	—	—	—	—	—	132.7 ± 2.0[d]
6	—	—	—	—	—	144.8 ± 2.0[d]
7	—	—	—	—	—	160.4 ± 1.6[d]
8	375–422	398.0	128.1 ± 1.0	73.5 ± 1.4	−66	134.5 ± 1.6[72]

[a] The standard Gibbs energies of vaporization were evaluated using the calibration coefficient developed in our recent work.[67] [b] From Table 4. [c] Adjusted to 298.15 K using the $\Delta_l^g C_{p,m}^\circ$ -values from (column 6). Uncertainties in the temperature adjustment of vaporization enthalpies from T_{av} to the reference temperature are estimated to account with 20% to the total adjustment. [d] Calculated as described in the text.

Table 4 Compilation of data on molar heat capacities $C^{\circ}_{p,m}$ and heat capacity differences [J K^{-1} mol^{-1}] at 298.15 K

Compound	$C^{\circ}_{p,m}$ (l)	$\Delta^{g}_{l}C^{\circ}_{p,m}$ [a]
1-NTf$_2$	605.7[c]	−89
2-NTf$_2$	622.9[b]	−93
3-NTf$_2$	718.6[b]	−118
[BMIm][NTf$_2$]	565.4[73]	—
[C_6Py][NTf$_2$]	612.0[74]	—

[a] Calculated by eqn (1). [b] Values of $C^{\circ}_{p,m}$(l, 298.15 K) of the imidazolium family were calculated based on the experimental value $C^{\circ}_{p,m}$(l, 298.15 K), [BMIm][NTf$_2$]) = 565.4 J K^{-1} mol^{-1} and group-contributions for the alkyl chain.[70,73] The specific increment [substituted imidazolium ring][NTf$_2$] = 399.9 J K^{-1} mol^{-1} has been defined. [c] Values of $C^{\circ}_{p,m}$(l, 298.15 K) of the pyridinium-based ILs were calculated from the experimental value $C^{\circ}_{p,m}$(l, 298.15 K), [C_6Py][NTf$_2$]) = 612 J K^{-1} mol^{-1} and the group-contributions for an alkyl chain.[73,74] The specific increment [*N*-substituted pyridinium][NTf$_2$] = 417.6 J K^{-1} mol^{-1} has been defined.

ments of vaporization enthalpies according to eqn (1) are compiled in Table 4.

Structure–property relationships in molecular and ionic compounds

Vaporization enthalpy is the bulk thermophysical property related to the whole scope of intermolecular interactions. For the molecular compounds the $\Delta^{g}_{l}H^{\circ}_{m}$(298.15 K) -value generally reflects the energetics of the van der Waals interactions among molecules in the liquid phase (provided that hydrogen bonding is absent in the molecular compound under consideration). For the ILs, the specific Coulomb forces additionally contribute to the overall interactions of molecules in the liquid phase. Thus, in contrast to the molecular liquids, the vaporization behavior of an IL is generally stipulated by the interplay of the van der Waals and Coulomb interactions. Introduction of a heteroatom like selenium within the alkyl chain of any molecular or ionic compound could additionally impact the interplay of intermolecular interaction in the liquid phase of the selenium-containing compound, and, as a consequence, the amount of vaporization enthalpy should indicate the extent of changes introduced by the selenium unit. In this context, it is interesting to compare vaporization enthalpies of the selenoether-functionalized ILs **1**- to **3-NTf$_2$** studied in this work with the vaporization enthalpies of a structurally similar ILs where the selenium atom is exchanged with the CH_2 fragment (see ILs **5–7**). Such a comparison will help to quantify the energetic extent of introduction of the Se-unity in the alkyl chain of the imidazolium cation. The vaporization enthalpies of the selenium-containing ILs **1** to **3-NTf$_2$** studied in this work are given in Table 3 (column 7), but unfortunately the experimental vaporization enthalpies $\Delta^{g}_{l}H^{\circ}_{m}$(298.15 K) of the comparable ILs **5–7** are absent in the literature. Nevertheless, the required values for ILs **5–7** can be reliably derived from the available data on the *N*-phenyl-*N*′-butylimidazolium-, **4** based and the *N*-propylpyridinium-, **8** based ILs with the common [NTf$_2$]-anion (Fig. 4). The experimental vaporization enthalpies $\Delta^{g}_{l}H^{\circ}_{m}$(298.15 K) of the ILs **4** and **8** have been reported in our earlier work and are given in Table 3.[72,75] However, the structures of the compounds **4** and **8** are only partially similar to the desired structures of the ILs **5–7** intended for the comparison. In order to derive the vaporization enthalpies of these ILs we combined the experimental vaporization enthalpies $\Delta^{g}_{l}H^{\circ}_{m}$(298.15 K) of the ILs **4** and **8** with the group-additivity (GA) procedure as follows. Indeed, in our recent study of ionic compounds (substituted *N*-phenylimidazolium-based ILs) and similarly shaped molecular compounds we have shown that the group-additivity parameters well-established for prediction of vaporization enthalpies of molecular compounds are generally transferable to the estimation of vaporization enthalpies of the ionic compounds.[75] This knowledge helps to combine the experimental vaporization enthalpies of the ILs **4** and **8** with the group-contribution values specific for molecular liquids (*e.g.* alkanes and alkylbenzenes) in order to assess the $\Delta^{g}_{l}H^{\circ}_{m}$(298.15 K)-values of the model compounds **5–7**, desired for comparison with those of the selenium-containing ILs. In order to set an example, let us consider the model compound **4** with the well-established value $\Delta^{g}_{l}H^{\circ}_{m}$(298.15 K) = (137.9 ± 2.0) kJ mol^{-1} (Table 3). In order to derive the enthalpy of vaporization of the IL **6**, we need to pull out the phenyl substituent from IL **4** and insert in-between two

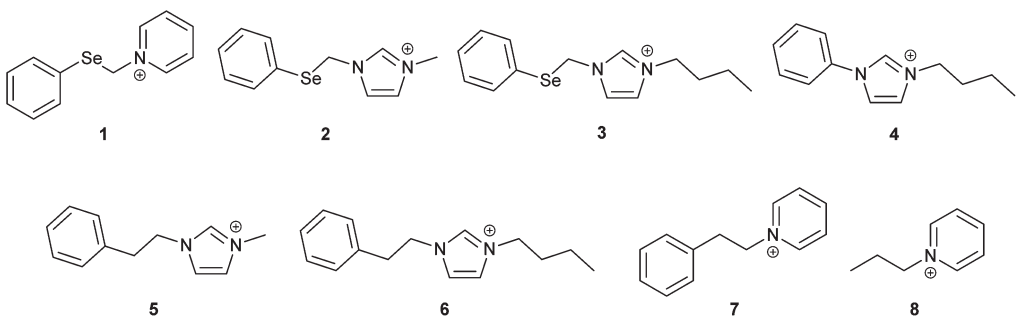

Fig. 4 Structures of the cations of the selenoether-funtionalized ILs **1–3**, of the aryl containing ILs **5–7** (taken for comparison with the selenium-containing ILs) and of the *N*-butyl-*N*′-phenylimidazolium cation **4** and *N*-propylpyridinium cation **8** (used for group-additivity calculations). The cations **4–8**, which are discussed in this work, were combined with the common [NTf$_2$]-anion for comparison with the selenoether-functionalized ILs **1–3-NTf$_2$**.[71]

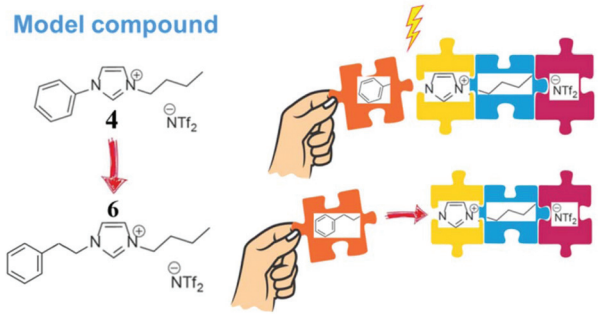

Fig. 5 Scheme of the procedure for the estimation of the $\Delta_l^g H_m^\circ$(298.15 K)-value for the IL **4**, starting with the experimental vaporization enthalpy of the model compound *N*-butyl-*N*′-phenylimidazolium bis(trifluoromethanesulfonyl)-imide **4**.

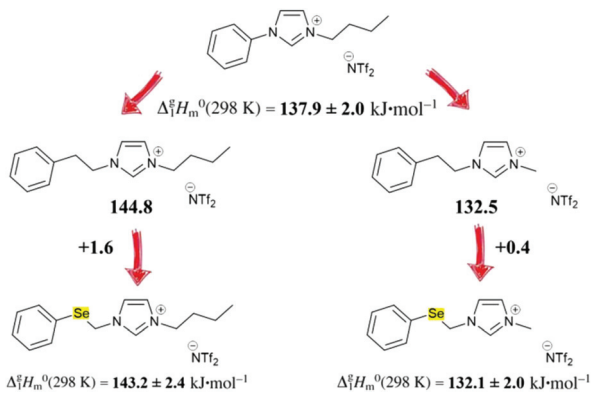

Fig. 6 Comparison of the vaporization enthalpies, $\Delta_l^g H_m^\circ$(298.15 K), in kJ mol^{-1} (given below for each molecule) of the imidazolium-based ILs (left is the comparison of IL **2** and **6** and right is the comparison of IL **1** and **5**).

groups CH_2–(N,C) = 3.17 kJ mol^{-1} and CH_2–(C_b,C) = 3.78 kJ mol^{-1} (the numeric values for the contributions to vaporization enthalpy due to inserting of groups CH_2–(N,C) and CH_2–(C_b,C) have been parametrized recently).[76] The resulting value $\Delta_l^g H_m^\circ(298.15\ \text{K}) = (137.9 + 3.17 + 3.78) = (144.8 \pm 2.0)$ kJ mol^{-1} (Table 3) for IL **6** can now be used for comparison with the vaporization enthalpy of the selenoether-functionalized IL **3-NTf$_2$**, as it is shown in Fig. 5. In the similar way, starting with IL **4**, adding of CH_2–(N,C) and CH_2–(C_b,C) groups at the left part and subtracting CH_2–(N,C) and 2 × CH_2–(2C) groups at the right side, the resulting value $\Delta_l^g H_m^\circ(298.15\ \text{K}) = (132.5 \pm 2.0)$ kJ mol^{-1} (Table 3) for IL **5** was calculated and it can now be used for comparison with the vaporization enthalpy of the selenoether-functionalized IL **2-NTf$_2$**, as shown in Fig. 6.

Starting with the pyridinium-based IL **8** with $\Delta_l^g H_m^\circ(298.15\ \text{K}) = (134.5 \pm 1.6)$ kJ mol^{-1}, subtracting the CH_3–(3C) contribution and adding the contribution for the phenyl ring [5 × C_bH–(2C_b) + C_b–(2C_b,C)] the resulting value $\Delta_l^g H_m^\circ(298.15\ \text{K}) = (160.4 \pm 1.6)$ kJ mol^{-1} (Table 3) for IL **7** was derived and used for comparison (Fig. 7) with the vaporization enthalpy of the selenium-containing IL **1-NTf$_2$**.

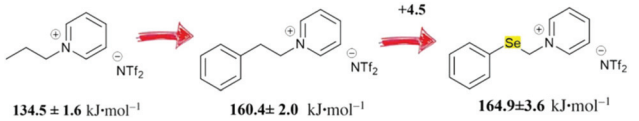

Fig. 7 Comparison of vaporization enthalpies, $\Delta_l^g H_m^\circ$(298.15 K), in kJ mol^{-1} (given below for each molecule) of the pyridinium-based ILs **3** and **7**).

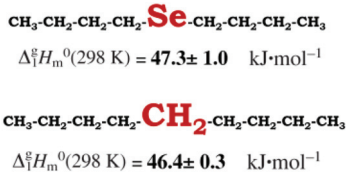

Fig. 8 Comparison of vaporization enthalpies, $\Delta_l^g H_m^\circ$(298.15 K), in kJ mol^{-1} (given below for each molecule) for dibutyl-selenide[77] and *n*-nonane.[78]

It is apparent from Fig. 6 and 7, that differences between the vaporization enthalpy $\Delta_l^g H_m^\circ$(298.15 K) of each selenium-containing IL **1-** to **3-NTf$_2$** and the vaporization enthalpy $\Delta_l^g H_m^\circ$(298.15 K) of the corresponding analogous CH_2-containing ILs (**5–7**) are hardly distinguishable (within their experimental uncertainties) for all three pairs taken for comparison.

Due to the limited vaporization enthalpy data available it is not possible to draw similarly safe conclusions for molecular selenium-containing compounds. Nevertheless, the comparison of the $\Delta_l^g H_m^\circ$(298.15 K) value available for di-butyl selenide with the vaporization enthalpy of a structurally analogous "CH_2-containing" compound *n*-nonane (Fig. 8) reveals that the contribution to the vaporization enthalpy through the introduction of a selenium atom into the alkyl chain can be suggested to be equal to those of the CH_2-group, both for the molecular compounds and ILs. This observation opens the way for reliable assessment of the $\Delta_l^g H_m^\circ$(298.15 K) for selenoether-functionalized ILs based on the available vaporization enthalpies of imidazolium, pyridinium or pyrrolidinium-based ILs with the help of group contributions derived from the molecular compounds. Vaporization enthalpies are commonly used for an assessment of a mutual solubility of different molecular or ionic compounds, making this data important for synthesis of materials *e.g.* in ILs.

Solubility parameters of the selenoether-functionalized ILs with [NTf$_2$]-anion

The solvation powers of solvents are conventionally predicted by the Hildebrand solubility parameters. The solubility parameters are generally the numerical values that indicate the strength of the intermolecular interactions between solute and solvent molecules. The solubility parameters have been widely used in many practical applications. This concept is useful for selecting a suitable composition of a solvent and a solute because the possible miscibility is indicated by similar

numerical values of the solubility parameters. The Hildebrand or total solubility parameter (δ_T) is defined by eqn (2),[79]

$$\delta_T = [(\Delta_l^g H_m^\circ - RT)/V_m]^{0.5} \quad (2)$$

where V_m is the molar volume, $\Delta_l^g H_m^\circ$ is the standard molar enthalpy of vaporization, R is the ideal gas constant, and T is the temperature. The vaporization enthalpies, $\Delta_l^g H_m^\circ$ and $\Delta_l^g C_{p,m}^\circ$ -values, required for calculations of δ_T of the selenoether-functionalized ILs at any temperature of interest have been developed in this work (Table 3). Values of the density temperature dependences measured in this work are given in Table S12.†

The solubility parameters, calculated according to eqn (2), are given in Table 5. Having established the solubility parameters of the selenium-containing ILs **1-** to **3-NTf$_2$** and the solvents (dichloromethane, acetone, *etc*. herein), one can easily calculate the Flory–Huggins interaction parameters x_{12} at infinite dilution, required for the assessment of the miscibility of any solute in ILs, according to eqn (3),[80]

$$x_{12} = \frac{V_1^*(\delta_1 - \delta_2)^2}{RT} \quad (3)$$

where δ_2 is the solubility parameter of the IL and δ_1 is the solubility parameter of the solute, R denotes the universal gas constant, T is the temperature, V_1* is the molar volume of the solute.

Values of the solubility parameters δ_1 and δ_2 have been calculated according to eqn (2) with the help of experimental data on vaporization enthalpies and densities for the solutes (taken from ref. 81 and for the solvents (selenium-containing ILs **1**–**3**) taken from Table 3.

Table 5 Flory-Huggins interaction parameters, x_{12} at infinite dilution of different solutes in the selenoether-functionalized ILs at 298 K and at 323 K

Solute	T/K	**1-NTf$_2$** [a] x_{12}	**2-NTf$_2$** [b] x_{12}	**3-NTf$_2$** [c] x_{12}
Dichloromethane	298	0.3	0.1	0.1
	323	0.4	0.1	0.1
Chloroform	298	0.7	0.1	0.1
	323	0.8	0.1	0.1
Acetone	298	0.4	0.1	0.1
	323	0.5	0.1	0.1
Acetonitrile	298	0.3	1.2	1.7
	323	0.1	0.9	1.2
Benzene	298	0.8	0.1	0.1
	323	0.9	0.2	0.2
n-Hexane	298	3.6	1.7	1.2
	323	3.6	1.8	1.4
Water	298	44	52	55
	323	39	46	49

[a] For **1-NTf$_2$**: V_m(298.15 K) = 330.3 cm^3 mol^{-1} and $\delta_{298.15\ K}$ = 22.2 MPa$^{0.5}$; V_m(323.15 K) = 336.4 cm^3 mol^{-1} and $\delta_{323.15\ K}$ = 21.8 MPa$^{0.5}$. [b] For **2-NTf$_2$**: V_m(298.15 K) = 325.3 cm^3 mol^{-1} and $\delta_{298.15\ K}$ = 20.0 MPa$^{0.5}$; V_m(323.15 K) = 329.9 cm^3 mol^{-1} and $\delta_{323.15\ K}$ = 19.6 MPa$^{0.5}$. [c] For **3-NTf$_2$**: V_m(298.15 K) = 379.9 cm^3 mol^{-1} and $\delta_{298.15\ K}$ = 19.2 MPa$^{0.5}$; V_m(323.15 K) = 385.6 cm^3 mol^{-1} and $\delta_{323.15\ K}$ = 18.9 MPa$^{0.5}$.

Modelling with ePC-SAFT

The procedure for ePC-SAFT modelling of ILs follows the strategy established in a prior work and will not be discussed in detail.[52] Briefly, ePC-SAFT uses an ion-based approach in which IL-ions interactions caused by hard-chain repulsion, van-der-Waals attraction and electrostatics are explicitly accounted for. Three pure-component parameters for each IL-ion are required for ePC-SAFT modelling; the segment number m^{seg}, the segment diameter σ as well as the dispersion-energy parameter u/k_B with the Boltzmann constant k_B. In general, these parameters are fitted directly to thermodynamic properties that are easily measured, and for ILs these are typically pure–component densities.

Since in the previous work the parameters of the [NTf$_2$]-anion have already been obtained, only the IL-cation parameters were fitted to experimental densities of the three ILs at different temperatures under atmospheric pressure. As the pure IL **2-NTf$_2$** was too viscous for density measurements using the equipment from Anton Paar, mixtures of acetonitrile and **2-NTf$_2$** were prepared, and mixture densities were measured (Table S12†). The fitted ePC-SAFT parameters for the IL-cations are listed in Table 6 together with the corresponding ARDs between ePC-SAFT modelled densities and experimental values. The respective density plot is shown in Fig. 9.

Table 6 ePC-SAFT pure-component parameters for IL-ions of the selenoether-functionalized ILs considered in this work

IL-ion	M_W	m	σ [Å]	u/k_B	ARD
IL-cation					
1	249.195	5.1443	3.2862	266.4032	0.09%
2	252.199	6.7780	3.2013	773.0798	0.76%
3	294.280	3.5598	4.4858	890.3716	0.07%
IL-anion					
[NTf$_2$][a]	280.145	6.0103	3.7469	375.6529	

[a] Taken from ref. 52, ARD $= 100 \times \frac{1}{NP}\sum_{i=1}^{NP}\left|1 - \frac{\rho^{calc}}{\rho^{exp}}\right|$.

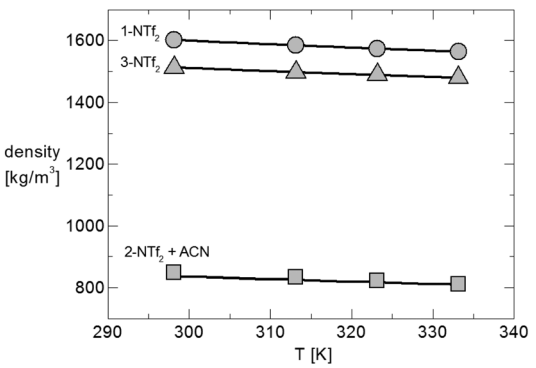

Fig. 9 Density of the pure selenoether-functionalized ILs **1-NTf$_2$** and **3-NTf$_2$** as well as the mixture density of **2-NTf$_2$** with acetonitrile (14.78 wt% IL). Symbols: experimental data; lines: ePC-SAFT modelling results.

Table 7 Comparison of experimental IL solubility in solvents and ePC-SAFT prediction results[a]

	ePC-SAFT	Experiment[c]
IL + water	Immiscible[b]	Immiscible
IL + *n*-hexane	Immiscible[b]	Immiscible
IL + acetone	Completely miscible	Miscible
IL + acetonitrile	Completely miscible	Miscible
IL + benzene	Completely miscible	Miscible
IL + chloroform	Completely miscible	Miscible
IL + DMSO	Completely miscible	Miscible

[a] ePC-SAFT predictions with IL-ion parameters from Table 6 using isofugacity approach. [b] The weight fraction of IL was predicted to be $<10^{-8}$. [c] 1 volume equivalent IL was mixed with 3 equivalents of solvent.

Based on the obtained parameters for the IL-ions, it was predicted with ePC-SAFT whether the ILs and classical solvents are miscible or not. Water and six different organic solvents were studied. For all solvents, the required ePC-SAFT parameters are available from the literature. No binary interaction parameters were applied for these predictions, *i.e.* the miscibility is predicted *in silico*. The results are listed in Table 7.

The results are in complete agreement with the experimental data. For both, *n*-hexane and water, the experimentally found immiscibility was also predicted with ePC-SAFT. Please note, that quantitative solubility data were not measured in this work. Further, ePC-SAFT predicted complete miscibility of the three ILs with the organic solvents acetone, acetonitrile, benzene, chloroform, and dimethyl sulfoxide. This was also found by miscibility experiments carried out in this work.

Thus, ePC-SAFT can be successfully used to screen solvents for the family of selenoether-functionalized ILs based on pure-component parameters for IL-ions that were obtained from experimental density data.

Nanoparticle synthesis

In order to synthesize ZnSe nanoparticles (NPs) using the selenoether–functionalized ILs, two different approaches under microwave irradiation at or near 250 °C were investigated (Scheme 3). In Method A the nanoparticles were synthesized from zinc acetate dihydrate in the selenoether-functionalized IL. Thus, the IL as reaction medium was present in large excess. Method B used the non-functionalized IL [BMIm][NTf_2]

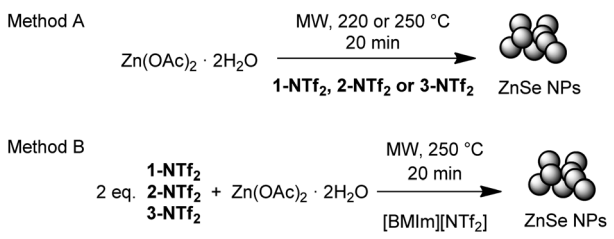

Scheme 3 Synthetic methodology for the synthesis of ZnSe nanoparticles directly in the functionalized IL (method A) and in [BMIm][NTf_2] (method B).

as a reaction medium, whereas the selenoether-functionalized IL was used as a near-stoichiometric selenium reagent with zinc acetate. The synthesis of ZnSe was chosen as a model compound since ZnSe NPs are well studied, air stable and stoichiometrically well defined.

In all cases ZnSe NPs with a cubic crystal structure and an average diameter below 10 nm could be observed, as verified by transmission electron microscopy (TEM) (Fig. 10), energy dispersive X-ray (EDX) spectroscopy and powder X-ray diffraction (PXRD). The average particle diameters from TEM match the crystallite sizes calculated from the respective powder patterns (Fig. 11 and 12) using the Scherrer equation with a Scherrer factor of 1 (Table 8). The TEM images of the nanoparticles obtained by method A exemplified for compound

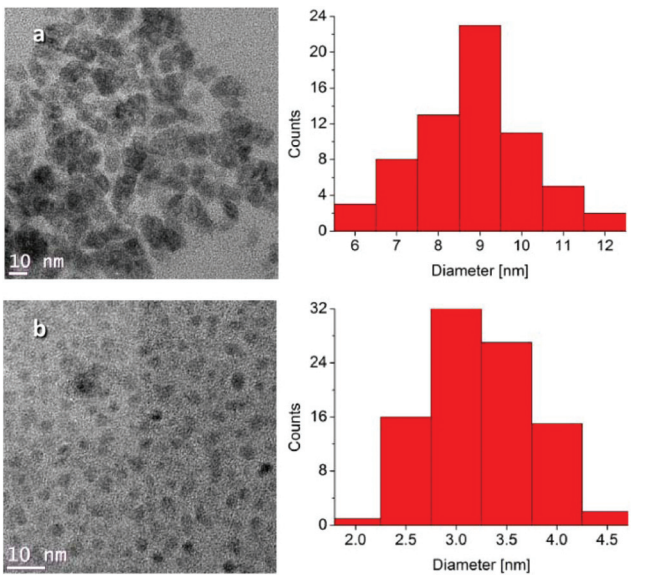

Fig. 10 Transmission electron microscopy (TEM) images and particle diameter distribution of ZnSe nanoparticles obtained by method A (a) and method B (b) from the selenoether-functionalized IL **2-NTf$_2$** (further TEM images and EDX-spectra are given in Fig. S46 and S47†).

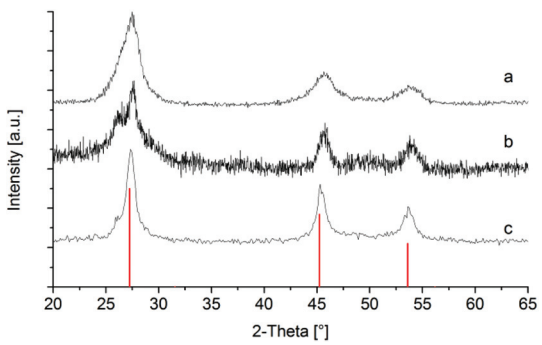

Fig. 11 Powder X-ray diffraction pattern of the ZnSe nanoparticles prepared according to method A directly in the selenoether-functionalized ILs (**1-NTf$_2$** (a), **2-NTf$_2$** (b), **3-NTf$_2$** (c) and reference simulation for cubic ZnSe (COD-ID: 9008879)).

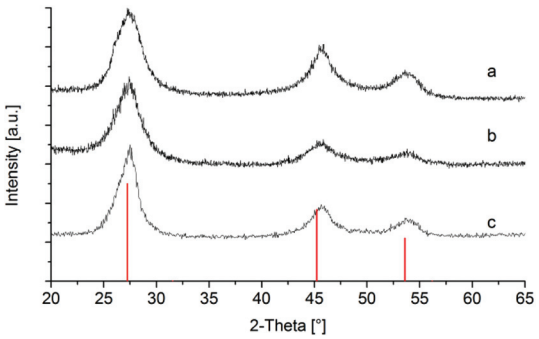

Fig. 12 Powder X-ray diffraction pattern of the ZnSe nanoparticles prepared according to method B in [BMIm][NTf_2] by reaction with two equivalents of **1-NTf_2** (a), **2-NTf_2** (b), **3-NTf_2** (c) and reference simulation for cubic ZnSe (COD-ID: 9008879).

Table 8 Results of the microwave-assisted synthesis of ZnSe nanoparticles from selenoether-functionalized ILs

	IL	Ø (TEM)[a] [nm]	Ø (XRD) [nm]
Method A	**1-NTf_2**	5 ± 2	4
	2-NTf_2	9 ± 3	11
	3-NTf_2	6 ± 2	6
Method B	**1-NTf_2**	6 ± 2	4
	2-NTf_2	3 ± 1	4
	3-NTf_2	6 ± 1	4

[a] Approximate width of diameter distribution covering about 90% of the particles from smallest to largest particle.

2-NTf_2, give an average diameter of 5–10 nm (Fig. 10 and S46†). The TEM images of the particles obtained by method B (Fig. 10 and S47†) yield an average diameter of 3–6 nm. This indicates that the exchange of the reaction medium has a certain effect on the particle size, presumably by influencing the nucleation and growth rate. This corresponds to known studies which have shown that the size of nanoparticles during the synthesis in ILs is essentially determined by the anion and that the effect of the cation appears to be relatively limited.[22,82,83]

Regarding the decomposition mechanism of the selenoether–functionalized ionic liquids and the formation of zinc selenide nanoparticles, we note that the formation of elemental selenium was not observed by microwave irradiaiton to 250 °C when using the selenoether-functionalized ILs as solvents (method A). Hence, there is no IL decomposition induced at this temperature. Therefore, we suggest that coordination of the selenoether functionality to the zinc cation is a prerequisite for a polarization and weakening of the selenium–carbon bond. Selenium is considered a soft Lewis base,[84] whereas Zn^{2+} is intermediate between a strong and weak Lewis acid. In the case of the selenoether-functionalized imidazolium ILs, the *in situ* formation of a carbene precursor complex appears to be a distinct possibility to induce the Zn–Se coordination by the spatial vicinity.[85]

Conclusions

Three selenoether-functionalized ILs with the bis(trifluoromethanesulfonyl)imide ([NTf_2]) anion were synthesized and their vaporization enthalpies and densities were determined. With regard to the vaporization enthalpies of the produced ILs, it could be shown on the basis of structure–property relationships between selenium-containing and similarly formed aryl-substituted imidazolium- and pyridinium-based ILs that the contribution of the Se-moiety to the enthalpy of vaporization of an IL is equal to the contribution of the methylene group. An incremental approach for the prediction of vaporization enthalpy of ILs by means of a group-contribution method was developed for this purpose, which is based on the vaporization enthalpy of an initial IL and respective group contributions, which are known from molecular compounds.

Based on their experimentally determined densities and vaporization enthalpies, their miscibility with classical solvents such as water, *n*-hexane or toluene was predicted both conventionally using Hildebrand solubility parameters and by modelling the ILs using the fully predictive method ePC-SAFT. The results of both methods correspond to the experimental miscibility observations.

Furthermore, it was shown that selenoether-functionalized ILs could be used for the synthesis of ZnSe nanoparticles (with cubic crystal structure) in a microwave-assisted synthesis. In all cases, ZnSe nanoparticles below 10 nm could be obtained without the need of other stabilizing agents besides the functionalized IL or [BMIm][NTf_2].

ePC-SAFT as well as the incremental approach for modelling the vaporization enthalpies of ILs demonstrated to be useful tools for the predictive screening of new ILs. However, further investigations, such as the quantitative prediction of phase equilibria or the contribution of other functional groups to the vaporization enthalpy, must be carried out.

Experimental section

General Remarks

Standard Schlenk techniques under inert gas atmosphere (N_2) were used for the syntheses of the ILs. Ethanol, tetrahydrofurane, dichloromethane and diethylether were dried over molecular sieves 3 Å. Diphenyldiselenide 96% and buthylimidazole 98% was purchased from TCI, sodium borohydride 99.99% and sodium tetraphenylborate 99.9% from Merck, methylimidazole 99% from Fluorochem and pyridine from Fluka. The IL [BMIm][NTf_2] was prepared according to literature procedures by the reaction of 1-methylimidazole with 1-chlorobutane in acetonitrile at 60 °C for three days. The reaction was followed by ion exchange with Li[NTf_2] in water and an additional extractive treatment.

Instrumentation

^{1}H-, ^{13}C- and ^{77}Se-NMR spectra were measured on an Avance III-600 or a Bruker Avance III-300 NMR-spectrometer at 298 K.

For the ^{77}Se-NMR-measurements a standard solution of KSeCN in D_2O was used.

The melting points of the prepared compounds were determined at a Büchi melting point apparatus B-540.

ESI-Mass-spectra were measured on a Finnigan LCQ Deca Ion-Trap-API-mass-spectrometer in positive and negative ion mode.

Thermal analyses were performed on a NETZSCH TG Tarsus 209 F3 with a heating rate of 5 K min^{-1} under N_2 atmosphere.

The purity of >99% of the ILs was assessed by ion chromatography (Dionex ICS-1100, with IonPac® AS22, 4 × 250 mm column).

The measurements for the pure-component densities of **1-NTf$_2$** and **3-NTf$_2$** as well as the densities of mixtures acetonitrile + **2-NTf$_2$** were performed using the oscillating U-tube apparatus DMA 4200 (Anton Paar GmbH, Graz, Austria) with a maximum uncertainty of ±1.5 × 10^{-6} g cm^{-3} calibrated with deionized water at atmospheric pressure.

The synthesis of the nanoparticles was carried out by decomposition of the precursors in a CEM Discover microwave reactor system.

The measurements of the powder patterns were done at room temperature on a Bruker D2 phaser in 2-theta angles with Cu-Kα-radiation (λ = 1.54182 Å) at a voltage of 35 kV.

The TEM images as well as the EDX-spectra were acquired with an FEI Tecnai G2 F20 operated at an accelerating voltage of 200 kV.[86] For TEM-EDX the exposure time for individual EDX spectra was 3 min (The EDX analyses always showed traces of oxygen as a result of the preparation of the grids in air).

X-ray crystallography

The single-crystal X-ray structure data were collected on a Bruker Kappa Duo APEX-II with CCD area-detector, Mo-Kα radiation (λ = 0.71073 Å), microfocus tube, multilayer mirror, ω and ϕ-scan scan; data collection with Apex2,[87] cell refinement and data reduction with SAINT, experimental absorption correction with SADABS.[88] Structure solution by direct methods using SHELXS-97; refinement by full-matrix least squares on F^2 using the SHELXL-97 program suite.[89] All non-hydrogen positions were refined with anisotropic displacement parameters. Hydrogen atoms on carbon atoms were positioned geometrically (with C–H = 0.95 Å for aromatic CH, C–H = 0.98 Å for CH_3, and C–H = 0.99 for CH_2) and refined using riding models (AFIX 43, 137 and 23, respectively) with U_{iso}(H) = 1.2U_{eq} and U_{iso}(H) = 1.5U_{eq}. Details of X-ray structure determination and data refinement are provided in Table S2.† Graphics were drawn with DIAMOND (Version 4.4.0).[90] The structural data has been deposited with the Cambridge Crystallographic Data Center under deposition numbers CCDC 1589574–1589576.†

Measurements of vaporization enthalpies by the quartz crystalline microbalance (QCM)

The absolute vapor pressures and the standard molar enthalpies of vaporization of the Se–ILs series were determined using the QCM method.[91] The vaporization enthalpies were derived from the temperature dependences of the experimentally measured change in the vibrational frequency of the quartz crystal. In the QCM method a sample of an IL is placed in an open cavity (Langmuir evaporation) inside of the thermostated block and it is exposed to vacuum (10^{-5} Pa) with the whole open surface of the loaded compound. The QCM sensor is placed directly above the measuring cavity containing the sample. During the vaporization into vacuum, a certain amount of sample is deposited on the quartz crystal. The change of the vibrational frequency Δf was directly related to the mass deposition Δm on the crystal according to the Sauerbrey equation (eqn (4)),[92]

$$\Delta f = -C \cdot f^{\,2} \cdot \Delta m \cdot S_C^{\,-1} \tag{4}$$

where f is the fundamental frequency of the crystal (6 MHz in this case) with $\Delta f \ll f$, S_C is the surface of the crystal, and C is a constant.[67] The measured frequency change rates (df/dt) can be used for calculation of absolute vapor pressures p_s according to eqn (5),

$$p_s = K' \frac{df}{dt} \sqrt{\frac{T}{M}} \tag{5}$$

where K' = (9.5 ± 1.1) × 10^{-6} Pa s kg$^{1/2}$ Hz^{-1} K$^{-1/2}$ mol$^{-1/2}$ is the empirical constant containing all parameters of the Sauerbrey equation as well as parameters specific for the geometry of the experimental setup.[67] The K'-value for our apparatus was evaluated with the help of reliable vapor pressure data on imidazolium- and pyridinium-based ILs compiled in references.[67] Using the frequency change rate df/dt measured by the QCM the molar enthalpy of vaporization, $\Delta_l^g H_m^\circ(T)$ at experimental temperatures is obtained by eqn (6),

$$\ln\left(\frac{df}{dt}\sqrt{T}\right) = A' - \frac{\Delta_l^g H_m^\circ(T_0) - \Delta_l^g C_{p,m}^\circ T_0}{R}\left(\frac{1}{T} - \frac{1}{T_0}\right) + \frac{\Delta_l^g C_{p,m}^\circ}{R}\ln\left(\frac{T}{T_0}\right) \tag{6}$$

where A' is the empirical constant; T_0 appearing in eqn (6) is an arbitrarily chosen reference temperature, which we have set to 298.15 K in this study. The value $\Delta_l^g C_{p,m}^\circ = C_{p,m}^\circ(g) - C_{p,m}^\circ(l)$ is the difference between the molar heat capacities of the gaseous, $C_{p,m}^\circ(g)$, and the liquid phase, $C_{p,m}^\circ(l)$, respectively. The vaporization enthalpy $\Delta_l^g H_m^\circ$(298.15 K) at the reference temperature is calculated according to the Kirchhoff's equation (eqn (7)),

$$\Delta_l^g H_m^\circ(298.15\ \text{K}) = \Delta_l^g H_m^\circ(T_{av}) + \Delta_l^g C_{p,m}^\circ(298.15 - T_{av}) \tag{7}$$

where T_{av} is the average temperature of the temperature range of the QCM study. In order to detect and avoid any possible effect of impurities on the measured frequency loss rate ($df/d\tau$), a typical experiment was performed in a few consequent series with increasing and decreasing temperature steps. Every series consisted of 7 to 11 temperature points of mass loss rate determination. Several runs have been performed to test the

reproducibility of the results. The study was finished when the enthalpy of vaporization, $\Delta_l^g H_m^\circ(298.15\ K)$, obtained in the sequential runs by adjusting eqn (7) to the temperature dependent rates ($df/d\tau$) agreed within the assessed experimental uncertainty of about ±1 kJ mol^{-1}. In order to confirm the absence of decomposition of the IL under the experimental conditions, the residual IL in the crucible and the IL-deposit on QCM were analyzed by ATR-IR spectroscopy. As can be seen in Fig. S44–S46 of the ESI† no changes in the spectra have been detected for ILs **2-NTf$_2$** and **3-NTf$_2$**. Spectra of the IL **1-NTf$_2$** show some minor changes in comparison to the initial material, and the uncertainty of the vaporization enthalpy for this IL was multiplied by factor 2. Primary experimental results of the QCM studies are given in Table S13 in the ESI.†

N-[(Phenylseleno)methylene]pyridinium bromide (1-Br)

In a 250 mL Schlenk flask 12.79 g (35.7 mmol) of diphenyldiselenide were dissolved in a mixture of 30 mL of dry ethanol and 20 mL of dry THF. The resulting orange-yellow solution was then added slowly within 15 min to a suspension of 4.03 g $NaBH_4$ (106.5 mmol) in 250 mL of dry CH_2Cl_2 in a 500 mL Schlenk flask. The reaction mixture was stirred overnight to give a colourless suspension, which was then washed with 100 mL of each 1 mol L^{-1} HCl, water and brine. The organic phase was dried with $MgSO_4$ and the solvent was evaporated. Afterwards, one equivalent (85.68 mmol) of freshly distilled pyridine and one equivalent KBr (85.7 mmol) was added to the residue, which then was stirred for 3 days at room temperature and refluxed afterwards for one hour. After the reaction mixture was cooled to room temperature the solution was diluted into 300 mL dry Et_2O and stirred for an additional hour. The etherous solution was decanted and the raw product was dissolved in $CHCl_3$, filtered and allowed to stand for crystallization to give colourless plate-like crystals.

Yield: 51%; ^{1}H-NMR (600 MHz, $CDCl_3$): δ (ppm) = 6.61 (br. s, 2H, NCH_2, $^2J_{1H,77Se}$ = 17.2 Hz); 7.20–7.30 (m, 3H, CH_{ortho} + CH_{para}), 7.42 (t, 2H CH_{meta}, ^3J = 7.2 Hz); 7.88 (br. s, 2H, CH_{meta} pyridyl), 8.48 (br. s, 1H, CH_{para} (pyridyl), 9.19 (br. s, 2H, CH_{ortho} pyridyl); ^{13}C-NMR (150 MHz, $CDCl_3$): δ (ppm) = 56.25 (NCH_2, $^1J_{13C,77Se}$ = 97.4 Hz), 125.11 (C_{ipso}, $^1J_{13C,77Se}$ = 105.6 Hz), 127.74 (C_{meta}), 129.61 (C_{meta} pyridyl) 129.90 (C_{para}), 135.45 (C_{ortho}), 144.28 (C_{ortho} pyridyl), 145.75 (C_{para} pyridyl); ^{77}Se-NMR (114 MHz, $CDCl_3$): δ (ppm) = 493.19; ESI-MS (m/z): 250.0 ($[C_{12}H_{12}NSe]^+$); TGA (5 °C min^{-1}): decomp. (T_{onset}): 195 °C.

N-(Methyl)-*N*′-[(phenylseleno)methylene]imidazolium chloride (2-Cl)

In a 250 mL Schlenk flask 12.79 g (35.7 mmol) of diphenyldiselenide were dissolved in a mixture of 20 mL of dry ethanol and 20 mL of dry THF. The resulting orange-yellow solution was then added slowly within 15 min to a suspension of 4.03 g $NaBH_4$ (106.5 mmol) in 250 mL of dry CH_2Cl_2 in a 500 mL Schlenk flask. The reaction mixture was stirred overnight to give a colourless suspension, which was then washed with 100 mL of each 1 mol L^{-1} HCl, water and brine. The organic phase was dried with $MgSO_4$ and the solvent was evaporated. Afterwards, one equivalent (85.68 mmol) of freshly distilled *N*-methylimidazole was added to the residue, which then was refluxed for 4 h. After cooling at room temperature the solution was diluted into 300 mL dry Et_2O and stirred for an additional hour. The etherous solution was decanted and the viscous residue was dissolved in CH_2Cl_2. After filtration the solvent was evaporated and the product was dried under vacuum for several hours to give the colorless to yellowish product, which crystallizes upon standing.

Yield: 50–65%; ^{1}H-NMR (300 MHz, $CDCl_3$): δ (ppm) = 3.79 (s, 3H, NCH_3); 5.72 (s, 2H, NCH_2, $^2J_{1H,77Se}$ = 17.37 Hz); 7.08–7.17 (m, 3H, CH_{ortho} + CH_{para}); 7.19 (s, 1H CH═CH); 7.34–7.37 (m, CH_{meta}); 7.56 (s, 1H, CH═CH); 9.74 (s, 1H, NCHN); ^{13}C-NMR (75 MHz, $CDCl_3$): δ (ppm) = 36.39 (NCH3); 44.32 (NCH2, $^1J_{13C,77Se}$ = 94.08 Hz), 121.78 (CH═CH), 123.65 (CH═CH), 126.11 (C_{ipso}, $^1J_{13C,77Se}$ = 100.14 Hz), 128.92 (C_{para}), 129.61 (C_{meta}), 134.41 (C_{ortho}, $^2J_{13C,77Se}$ = 9.90 Hz), 136.70 (NCHN); ^{77}Se-NMR (114 MHz, $CDCl_3$): δ (ppm) = 434.13; ESI-MS (m/z): 253.0 ($[C_{11}H_{13}N_2Se]^+$); TGA (5 °C min^{-1}): decomp. (T_{onset}): 243 °C.

N-(Butyl)-*N*′-[(phenylseleno)methylene]imidazolium bromide (3-Br)

In a 250 mL Schlenk flask 12.79 g (35.7 mmol) of diphenyldiselenide were dissolved in a mixture of 20 mL of dry ethanol and 20 mL of dry THF. The resulting orange-yellow solution was then added slowly within 15 min to a suspension of 4.03 g $NaBH_4$ (106.5 mmol) in 250 mL of dry CH_2Cl_2 in a 500 mL Schlenk flask. The reaction mixture was stirred overnight to give a colourless suspension, which was then washed with 100 mL of each 1 mol L^{-1} HCl, water and brine. The organic phase was dried with $MgSO_4$ and the solvent was evaporated. Afterwards, one equivalent (85.7 mmol) of freshly distilled *N*-butylimidazole and 1 equivalent of KBr (85.7 mmol, 10.19 g) was added to the residue, which then was stirred for 3 days and refluxed afterwards for one hour. After the reaction mixture was cooled to room temperature the solution was diluted into 300 mL dry Et_2O and stirred for an additional hour. The etherous solution was decanted and the viscous residue was dissolved in CH_2Cl_2. After filtration the solvent was evaporated and the product was dried under vacuum for several hours to give the colorless to yellowish product, which crystallizes upon standing.

Yield: 83%; ^{1}H-NMR (300 MHz, $CDCl_3$): δ (ppm) = 0.78 (t, 3H, CH_3, ^3J = 7.3 Hz), 1.09 (sxt, 2H, $\underline{CH_2}CH_3$, ^3J = 7.5 Hz), 1.64 (quin., 2H, $\underline{CH_2}CH_2CH_3$, ^3J = 7.5 Hz) 4.08 (t, 2H, $N\underline{CH_2}CH_2$, ^3J = 7.2 Hz), 5.82 (s, 2H, NCH_2, $^2J_{1H,77Se}$ = 17.5 Hz); 7.17–7.21 (m, 3H, CH_{ortho} + CH_{para}), 7.38 (s, 1H CH═CH); 7.43–7.44 (m, CH_{meta}), 7.57 (s, 1H, CH═CH); 9.90 (s, 1H, NCHN) ^{13}C-NMR (75 MHz, $CDCl_3$): δ (ppm) = 13.72 (CH_3), 19.10 ($\underline{CH_2}CH_3$), 31.86 ($\underline{CH_2}CH_2CH_3$) 44.18 (NCH_2, $^1J_{13C,77Se}$ = 93.5 Hz), 49.73 ($N\underline{CH_2}CH_2$), 122.02 (CH═CH), 122.33 (C_{ipso}), 125.81 (CH═CH), 129.08 (C_{para}), 129.75 (C_{meta}), 134.80 (C_{ortho}, $^2J_{13C,77Se}$ = 9.9 Hz), 136.16 (NCHN); ^{77}Se-NMR (114 MHz, $CDCl_3$): δ (ppm) = 440.72; ESI-MS: (m/z) = 295.1 ($[C_{14}H_{19}N_2Se]^+$); TGA (5 °C min^{-1}): decomp. (T_{onset}): 233 °C.

Synthesis of 1- to 3-NTf_2

The halide **1-Br**, **2-Cl** or **3-Br** (31.0 mmol) was dissolved in 50 mL of water in a 100 mL Schlenk flask. To this solution 8.89 g (31.0 mmol) of $Li[NTf_2]$ were added. The reaction mixture was stirred overnight at room temperature. The solvent was evaporated and the residue was stirred in 100 mL of CH_2Cl_2 for 2 hours. After filtration the resulting solution was washed with water until no chloride could be detected by reaction of the aqueous solution with $AgNO_3$. The etherous phase was dried with $MgSO_4$, the solvent evaporated and the product was dried in vacuum for several hours.

N-[(Phenylseleno)methylene]pyridinium bis (trifluoromethanesulfonyl)imide (1-NTf_2)

Yield: 83%; ^{1}H-NMR (600 MHz, $CDCl_3$): δ (ppm) = 5.84 (s, 2H, NCH_2, $^2J_{1H,77Se}$ = 17.3 Hz); 7.27 (t, 2H, CH_{ortho}, ^3J = 7.6 Hz) 7.35–7.39 (m, 3H, CH_{meta} + CH_{para}); 7.82 (t, 2H, CH_{meta} (Pyridin), ^3J = 7.0 Hz); 8.47 (t, 1H, CH_{para} (pyridyl), ^3J = 7.3 Hz); 9.18 (d, 2H, CH_{ortho} (pyridyl), ^3J = 5.8 Hz); ^{13}C-NMR (150 MHz, $CDCl_3$): 56.06 (NCH_2, $^1J_{13C,77Se}$ = 99.0 Hz), 119.44 (CF_3, $^1J_{13C,19F}$ = 321.3 Hz), 124.18 (C_{ipso}, $^1J_{13C,77Se}$ = 97.04 Hz), 129.96 (C_{meta}), 127.88 (C_{meta} (pyridyl)) 130.42 (C_{para}), 135.43 (C_{ortho}), 143.25 (C_{ortho} (pyridyl)), 145.91 (C_{para} (pyridyl)); ^{77}Se-NMR (114 MHz, $CDCl_3$): 492.95; ESI-MS (m/z) = 250.0 ($[C_{12}H_{12}NSe]^+$) or 279.9 ($[NTf_2]^-$); TGA (5 °C min^{-1}): decomp. (T_{onset}): 227 °C. Anal. calcd for $[C_{12}H_{12}NSe]$ $[C_2F_6N_2O_4]$ (529.34 g mol^{-1}): C 31.77, H 2.28, N 5.29, S 12.12, found: C 30.80, H 2.38, N 5.64, S 11.54%.

N-(Methyl)-*N*′-[(phenylseleno)methylene]imidazolium bis (trifluoromethanesulfonyl)imide (2-NTf_2)

Yield: 86%; ^{1}H-NMR (300 MHz, $CDCl_3$): δ (ppm) = 3.69 (s, 3H, NCH_3); 5.38 (s, 2H, NCH_2, $^2J_{1H,77Se}$ = 17.4 Hz); 7.14–7.48 (m, 7H, 2 × CH═CH, CH_{para}, CH_{meta}, CH_{ortho}), 8.23 (s, 1H, NCHN); ^{13}C-NMR (150 MHz, $CDCl_3$): 36.02 (NCH_3), 44.12 (NCH_2, $^1J_{13C,77Se}$ = 94.6 Hz), 119.44 (CF_3, $^1J_{13C,19F}$ = 320.5 Hz) 122.19 (CH═CH), 123.82 (CH═CH), 125.73 (C_{ipso}, $^1J_{13C,77Se}$ = 97.9 Hz), 129.58 (C_{para}), 129.88 (C_{meta}), 134.99 (C_{ortho}), 135.34 (NCHN); ^{77}Se-NMR (114 MHz, $CDCl_3$): 444.49; ESI-MS m/z = 253.0 ($[C_{11}H_{13}N_2Se]^+$) or 279.9 ($[NTf_2]^-$); TGA (5 °C min^{-1}) decomp. (T_{onset}): 285 °C. Anal. calcd for $[C_{11}H_{13}N_2Se][C_2F_6N_2O_4]$ (523.34 g mol^{-1}): C 29.33, H 2.46, N 7.89, S 12.05, found: C 29.08, H 2.64, N 7.64, S 11.74%.

N-(Butyl)-*N*′-[(phenylseleno)methylene]imidazolium bis (trifluoromethanesulfonyl)imide (3-NTf_2)

Yield: 78%; ^{1}H-NMR (300 MHz, $CDCl_3$): δ (ppm) = 0.78 (t, 3H, CH_3, ^3J = 7.3 Hz) 1.07 (sxt, 2H, $\underline{CH}_2CH_3$, ^3J = 7.6 Hz); 1.56 (quin., 2H, $\underline{CH}_2CH_2CH_3$, ^3J = 7.5 Hz) 3.92 (t, 2H, $N\underline{CH}_2CH_2$, ^3J = 7.3 Hz), 5.40 (s, 2H, NCH_2, $^2J_{1H,77Se}$ = 17.0 Hz); 7.16–7.30 (m, 5H, CH_{ortho} + CH_{para} + CH_{meta}), 7.34 (br. s, 1H CH═CH), 7.36 (br. s, 1H CH═CH), 8.23 (s, 1H, NCHN); ^{13}C-NMR (75 MHz, $CDCl_3$): 12.46 (CH_3), 18.45 ($\underline{CH}_2CH_3$), 31.18 ($\underline{CH}_2CH_2CH_3$), 43.39 (NCH_2, $^1J_{13C,77Se}$ = 93.5 Hz), 49.21 ($N\underline{CH}_2CH_2$), 119.33 (CF_3, $^1J_{13C,19F}$ = 321.3 Hz), 121.88 (CH═CH), 122.42 (CH═CH), 124.92 (C_{ipso}), 129.07 (C_{para}), 129.46 (C_{meta}), 134.18 (NCHN), 134.68 (C_{ortho},); ^{77}Se-NMR (114 MHz, $CDCl_3$): 442.84; ESI-MS (m/z) = 295.1 ($[C_{14}H_{19}N_2Se]^+$) 279.9 (NTf_2^-); TGA (5 °C min^{-1}) decomp. (T_{onset}): 285 °C. Anal. calcd for $[C_{14}H_{19}N_2Se][C_2F_6N_2O_4]$ (574.42 g mol^{-1}): C 33.45, H 3.33, N 7.32, S 11.16, found: C 33.58, H 3.53, N 7.33, S 11.20%.

Synthesis of 2-BPh_4 and 3-BPh_4

The halide **2-Cl** or **3-Br** (30 mmol) was dissolved in 50 mL of ethanol in a 100 mL Schlenk flask. To this solution an excess of sodium tetraphenylborate was added resulting in the immediate precipitation of sodium chloride or bromide respectively. The reaction mixture was stirred for one hour at room temperature. After the solvent was evaporated the desired product was extracted with 100 mL of CH_2Cl_2. After filtration the resulting solution was washed with water until no chloride could be detected by reaction of the aqueous solution with $AgNO_3$. The organic phase was allowed to stand for crystallization to give colourless crystals.

N-(Methyl)-*N*′-[(phenylseleno)methylene]imidazolium tetraphenylborate (2-BPh_4)

Yield: 68%; ^{1}H-NMR (600 MHz, DMSO-d_6): δ (ppm) = 3.76 (s, 3H, NCH_3), 5.74 (s, 2H, NCH_2, $^2J_{1H,77Se}$ = 17.3 Hz), 6.80 (t, 4H, CH_{para} (BPh_4), ^3J = 7.2 Hz), 6.93 (t, 8H, CH_{meta} (BPh_4), ^3J = 7.4 Hz) 7.17–7.21 (m, 8H, CH_{ortho} (BPh_4)), 7.35–7.41 (m, 3H, CH_{meta} + CH_{para}); 7.49 (d, 1H CH═CH, ^3J = 1.2 Hz), 7.51 (d, 1H CH═CH, ^3J = 1.3 Hz), 7.62 (dt, 2H, CH_{ortho}, ^3J = 8.7 Hz, ^4J = 1.8 Hz), 8.96 (s, 1H, NCHN); ^{13}C-NMR (150 MHz, DMSO-d_6): δ (ppm) = 35.88 (NCH_3); 34.51 (NCH_2, $^1J_{13C,77Se}$ = 91.3 Hz), 121.51 (CH_{para} (BPh_4)), 122.40 (CH═CH), 124.03 (CH═CH), 125.30 (CH_{meta} (BPh_4), $^3J_{13C,11B}$ = 2.8 Hz), 126.76 (C_{ipso}), 128.69 (C_{para}), 129.69 (C_{meta}), 133.70 (C_{ortho}, $^2J_{13C,77Se}$ = 9.90 Hz), 135.53 (CH_{ortho} (BPh_4)), 136.39 (NCHN), 163.4 ((CH_{ipso} (BPh_4), $^3J_{13C,11B}$ = 49.0 Hz); ^{77}Se-NMR (114 MHz, $CDCl_3$): δ (ppm) = 428.55; ESI-MS m/z = 253.0 ($[C_{11}H_{13}N_2Se]$ +) or 319.2 ($[BPh_4]^-$).

N-(Butyl)-*N*′-[(phenylseleno)methylene]imidazolium tetraphenylborate (3-BPh_4)

Yield: 78%; ^{1}H-NMR (300 MHz, $CDCl_3$): δ (ppm) = 0.86 (t, 3H, CH_3, ^3J = 7.3 Hz) 1.09 (sxt, 2H, $\underline{CH}_2CH_3$, ^3J = 7.4 Hz); 1.63 (quin., 2H, $\underline{CH}_2CH_2CH_3$, ^3J = 7.3 Hz) 4.07 (t, 2H, $N\underline{CH}_2CH_2$, ^3J = 7.0 Hz), 5.75 (s, 2H, NCH2, $^2J_{1H,77Se}$ = 17.7 Hz), 6.81 (t, 4H, CH_{para} (BPh_4), ^3J = 7.2 Hz), 6.94 (t, 8H, CH_{meta} (BPh_4), ^3J = 7.4 Hz) 7.19–7.24 (m, 8H, CH_{ortho} (BPh_4)), 7.33–7.40 (m, 3H, CH_{meta} + CH_{para}); 7.48–7.51 (m, 2H CH═CH); 7.70 (dt, 2H, CH_{ortho}, ^3J = 8.7 Hz, ^4J = 1.8 Hz) 9.05 (s, 1H, NCHN); ^{13}C-NMR (150 MHz, DMSO-d_6): δ (ppm) = 13.16 (CH_3), 18.53 ($\underline{CH}_2CH_3$), 31.21 ($\underline{CH}_2CH_2CH_3$), 43.47 (NCH_2Se), 48.59 ($N\underline{CH}_2CH_2$), 121.47 (CH_{para} (BPh_4)), 122.53 (CH═CH), 122.87 (CH═CH), 125.24 (CH_{meta} (BPh_4), $^3J_{13C,11B}$ = 2.9 Hz), 126.33 (C_{ipso}), 128.71 (C_{para}), 129.61 (C_{meta}), 133.97 (C_{ortho}), 135.50 (CH_{ortho} (BPh_4)), 135.81 (NCHN), 163.34 ((CH_{ipso} (BPh_4), $^3J_{13C,11B}$ = 49.0 Hz); ^{77}Se-NMR (114 MHz, DMSO-d_6): δ (ppm) = 427.19; ESI-MS (m/z) = 295.1 ($[C_{14}H_{19}N_2Se]^+$) or 319.2 ($[BPh_4]^-$).

Synthesis of the zinc-selenide nanoparticles

Method A

Suspensions of ~1 wt% ZnSe in the selenoether-functionalized ILs were obtained by suspending solid zinc acetate dihydrate (24 mg, 23 mg or 23 mg) in 1 mL of the IL **1-NTf$_2$**, **2-NTf$_2$** or **3-NTf$_2$**, respectively, under vacuum and decomposition under microwave-assisted heating (40 W) at 250 °C (220 °C for IL **1-NTf$_2$**) for 10 min. The gaseous by-products were removed under reduced pressure. For further analysis the particles were first precipitated with 1 mL of acetonitrile and then washed 4–5 times with 1 mL of acetonitrile each.

Method B

Suspensions of ~1 wt% ZnSe were obtained by stirring solid zinc acetate dihydrate (22 mg, 0.1 mmol) with two molar equivalents of the IL **1-NTf$_2$** (104 mg), **2-NTf$_2$** (106 mg) or **3-NTf$_2$** (114 mg), respectively, under vacuum. After one hour 1 mL (1.4 g) of [BMIm][NTf$_2$] was added and the reaction mixture was again stirred under vacuum until the zinc acetate was finely dispersed. The decomposition was carried out under microwave-assisted heating (40 W) at 250 °C for 10 min. The gaseous by-products were removed under reduced pressure and, identical to method A, the particles were precipitated and washed with acetonitrile for further analysis.

Conflicts of interest

There are no conflicts to declare.

Acknowledgements

This work has been supported by the German Science Foundation (DFG) in the frame of the priority program SPP 1807 "*Control of London Dispersion Interactions in Molecular Chemistry*" (grant DFG VE 265/10-1 for SV), as well as of the priority program SPP 1708 "*Material Synthesis Near Room Temperature*" (grant JA 466/31-1/2 for CJ, grant HE 7165/7-1 for CH and grant VE 265/14-1 for SV).

Notes and references

1 R. L. Vekariya, *J. Mol. Liq.*, 2017, **227**, 44–60.
2 Q. Zhang, S. Zhang and Y. Deng, *Green Chem.*, 2011, **13**, 2619–2637.
3 M. Koel, in *Analytical Applications of Ionic Liquids*, ed. M. Koel, World Scientific, Singapore, 2016.
4 T. D. Ho, C. Zhang, L. W. Hantao and J. L. Anderson, *Anal. Chem.*, 2014, **86**, 262–285.
5 J. Choi, T. M. Benedetti, R. Jalili, A. Walker, G. G. Wallace and D. L. Officer, *Chem. – Eur. J.*, 2016, **22**, 14158–14161; G. A. Elia, U. Ulissi, F. Müller, J. Reiter, N. Tsiouvaras, Y.-K. Sun, B. Scrosati, S. Passerini and J. Hassoun, *Chem. – Eur. J.*, 2016, **22**, 6808–6814; D. S. Silvester and R. G. Compton, *Z. Phys. Chem.*, 2006, **220**, 1247–1274.
6 G. Cui, J. Wang and S. Zhang, *Chem. Soc. Rev.*, 2016, **45**, 4307–4339.
7 S. P. Kelley, L. A. Flores, M. S. Shannon, J. E. Bara and R. D. Rogers, *Chem. – Eur. J.*, 2017, **23**, 14332–14337; L. Sun, G. K. Ramesha, P. V. Kamat and J. F. Brennecke, *Langmuir*, 2014, **30**, 6302–6308.
8 S. S. Moganty, P. S. Chinthamanipeta, V. K. Vendra, S. Krishnan and R. E. Baltus, *Chem. Eng. J.*, 2014, **250**, 377–389.
9 T. Brünig, K. Krekic, C. Bruhn and R. Pietschnig, *Chem. – Eur. J.*, 2016, **22**, 16200–16212; D. R. MacFarlane, N. Tachikawa, M. Forsyth, J. M. Pringle, P. C. Howlett, G. D. Elliott, J. H. Davis, M. Watanabe, P. Simon and C. A. Angell, *Energy Environ. Sci.*, 2014, **7**, 232–250.
10 S. Y. Lee, A. Ogawa, M. Kanno, H. Nakamoto, T. Yasuda and M. Watanabe, *J. Am. Chem. Soc.*, 2010, **132**, 9764–9773.
11 Y. Wang, S. Huang, W. Zhang, T. Liu, X. Qi and Q. Zhang, *Chem. – Eur. J.*, 2017, **23**, 12502–12509; Y. Bai, Y. M. Cao, J. Zhang, M. K. Wang, R. Z. Li, P. Wang, S. M. Zakeeruddin and M. Grätzel, *Nat. Mater.*, 2008, **7**, 626–630.
12 K. Klauke, B. Hahn, K. Schütte, J. Barthel and C. Janiak, *Nano-Struct. Nano-Objects*, 2015, **1**, 24–31.
13 M.-R. Gao, J. Yuan and M. Antonietti, *Chem. – Eur. J.*, 2017, **23**, 5391–5403; R. Marcos Esteban, K. Schütte, P. Brandt, D. Marquardt, H. Meyer, F. Beckert, R. Mülhaupt, H. Kölling and C. Janiak, *Nano-Struct. Nano-Objects*, 2015, **2**, 11–18.
14 M. Fischer, J. Schwegler, C. Paula, P. S. Schulz and M. Hartmann, *Dalton Trans.*, 2016, **45**, 18443–18446.
15 M. Abai, M. P. Atkins, A. Hassan, J. D. Holbrey, Y. Kuah, P. Nockemann, A. A. Oliferenko, N. V. Plechkova, S. Rafeen, A. A. Rahman, R. Ramli, S. M. Shariff, K. R. Seddon, G. Srinivasan and Y. Zoub, *Dalton Trans.*, 2015, **44**, 8617–8624.
16 D. W. Bruce, Y. Gao, J. N. Canongia Lopes, K. Shimizu and J. M. Slattery, *Chem. – Eur. J.*, 2016, **22**, 16113–16123; M. Antonietti, D. Kuang, B. Smarsly and Y. Zhou, *Angew. Chem., Int. Ed.*, 2004, **43**, 4988–4993.
17 R. A. Sheldon, *Chem. – Eur. J.*, 2016, **22**, 12983–12998; J. Alarcon-Esposito, R. Contreras, R. A. Tapia and P. R. Campodonico, *Chem. – Eur. J.*, 2016, **22**, 13347–13351; H. Zoua, Z. Lia, Y. Luan, T. Mu, Q. Wang, L. Li, J. Ge and G. Chen, *Curr. Opin. Solid State Mater. Sci.*, 2008, **12**, 1–8.
18 K. Schütte, A. Doddi, C. Kroll, H. Meyer, C. Gemel, G. van Tendeloo, R. A. Fischer and C. Janiak, *Nanoscale*, 2014, **6**, 5532–5544.
19 K. Schütte, H. Meyer, C. Gemel, J. Barthel, R. A. Fischer and C. Janiak, *Nanoscale*, 2014, **6**, 3116–3126.
20 S. Wolf, K. Reiter, F. Weigend, W. Klopper and C. Feldmann, *Inorg. Chem.*, 2015, **54**, 3989–3994.
21 S. Wegner, C. Rutz, K. Schütte, J. Barthel, A. Bushmelev, A. Schmidt, K. Dilchert, R. A. Fischer and C. Janiak, *Chem. – Eur. J.*, 2017, **23**, 6330–6340; C. Rizzo, F. D'Anna, R. Noto, M. Zhang and R. G. Weiss, *Chem. – Eur. J.*, 2016, **22**, 11269–11282.
22 J. Łuczak, M. Paszkiewicz, A. Krukowska, A. Malankowska and A. Zaleska-Medynska, *Adv. Colloid Interface Sci.*, 2016,

230, 13–28; J. Łuczak, M. Paszkiewicz, A. Krukowska, A. Malankowska and A. Zaleska-Medynska, *Adv. Colloid Interface Sci.*, 2016, **227**, 1–52; S. Wegner and C. Janiak, *Top. Curr. Chem. Z*, 2017, **375**, 65, DOI: 10.1007/s41061-017-0148-1; C. Janiak, *Z. Naturforsch. B*, 2013, **68**, 1056–1089.

23 S. Santner, S. Yogendra, J. J. Weigand and S. Dehnen, *Chem. – Eur. J.*, 2017, **23**, 1999–2004.

24 P. Wasserscheid and T. Welton, in *Ionic Liquids in Synthesis*, ed. P. Wasserscheid and T. Welton, Wiley-VCH Verlag GmbH & Co. KGaA, Weinheim, Germany, 2nd edn, 2007.

25 A. Alvarez Fernandez and P. H. J. Kouwer, *Int. J. Mol. Sci.*, 2016, **17**, 731–738.

26 B. Wang, L. Qin, T. Mu, Z. Xue and G. Gao, *Chem. Rev.*, 2017, **117**, 7113–7131.

27 L. Xu, W. Chen and J. Xiao, *Organometallics*, 2000, **19**, 1123–1127.

28 C. J. Mathews, P. J. Smith, T. Welton, A. J. P. White and D. J. Williams, *Organometallics*, 2001, **20**, 3848–3850.

29 J. Dupont and J. Spencer, *Angew. Chem., Int. Ed.*, 2004, **43**, 5296–5297.

30 S. Chowdhury, R. S. Mohan and J. L. Scott, *Tetrahedron*, 2007, **63**, 2363–2389.

31 H. L. Ngo, K. LeCompte, L. Hargens and A. B. McEwen, *Thermochim. Acta*, 2000, **97**, 357–358.

32 N. Meine, F. Benedito and R. Rinaldi, *Green Chem.*, 2010, **12**, 1711–1714.

33 R. E. Del Sesto, T. M. McCleskey, C. Macomber, K. C. Ott, A. T. Koppisch, G. A. Baker and A. K. Burrell, *Thermochim. Acta*, 2009, **491**, 118–120.

34 C. Maton, N. De Vos and C. V. Stevens, *Chem. Soc. Rev.*, 2013, **42**, 5963–5977.

35 N. D. De Vos, C. Maton and C. V. Stevens, *ChemElectroChem.*, 2014, **1**, 1258–1270.

36 D. M. Fox, W. H. Awad, J. W. Gilman, P. H. Maupin, H. C. De Long and P. C. Trulove, *Green Chem.*, 2003, **5**, 724–727.

37 A. Efimova, L. Pfützner and P. Schmidt, *Thermochim. Acta*, 2015, **604**, 129–136.

38 A. Efimova, G. Hubrig and P. Schmidt, *Thermochim. Acta*, 2013, **573**, 162–169.

39 K. Schütte, J. Barthel, M. Endres, M. Siebels, B. M. Smarsly, J. Yue and C. Janiak, *ChemistryOpen*, 2017, **6**, 137–148; A. Schmitz, K. Schütte, V. Ilievski, J. Barthel, L. Burk, R. Mülhaupt, J. Yue, B. Smarsly and C. Janiak, *Beilstein J. Nanotechnol.*, 2017, **8**, 2474–2483.

40 (*a*) C. Lorbeer, F. Behrends, J. Cybinska, H. Eckert and A.-V. Mudring, *J. Mater. Chem. C*, 2014, **2**, 9439–9450; (*b*) D. G. Archer, J. A. Widegren, D. R. Kirklin and J. W. Magee, *J. Chem. Eng. Data*, 2005, **50**, 1484–1491.

41 J. Olchowka, M. Suta and C. Wickleder, *Chem. – Eur. J.*, 2017, **23**, 12092–12095.

42 A. Taubert, F. Stange, Z. H. Li, M. Junginger, C. Günter, M. Neumann and A. Friedrich, *ACS Appl. Mater. Interfaces*, 2012, **4**, 791–795.

43 R. Li, Y. Luan, H. Zou, J. Du, T. Mu and Z. Li, *RSC Adv.*, 2012, **2**, 3049–3056.

44 Z. Li, Y. Luan, T. Mu and G. Che, *Chem. Commun.*, 2009, 1258–1260.

45 R. Göbel, Z.-L. Xie, M. Neumann, C. Günter, R. Löbbicke, S. Kubo, M.-M. Titirici, C. Giordano and A. Taubert, *CrystEngComm*, 2012, **14**, 4946–4951.

46 A. Taubert, *Angew. Chem., Int. Ed.*, 2004, **43**, 5380–5382.

47 M. Loor, G. Bendt, J. Schaumann, U. Hagemann, M. Heidelmann, C. Wölper and S. Schulz, *Z. Anorg. Allg. Chem.*, 2017, **643**, 60–68.

48 J. E. S. J. Reid, C. E. S. Bernardes, F. Agapito, F. Martins, S. Shimizu, M. E. Minas da Piedade and A. J. Walker, *Phys. Chem. Chem. Phys.*, 2017, **19**, 28133–28138.

49 D. H. Zaitsau, A. V. Yermalayeu, V. N. Emel'yanenko, C. Schick, S. P. Verevkin, A. A. Samarov, S. Schlenk and P. Wasserscheid, *Z. Phys. Chem.*, 2012, **227**, 205–216.

50 D. H. Zaitsau, M. A. Varfolomeev, S. P. Verevkin, A. D. Stanton, M. S. Hindman and J. E. Bara, *J. Chem. Thermodyn.*, 2016, **93**, 151–156.

51 T. L. Greaves and C. J. Drummond, *Chem. Rev.*, 2015, **115**, 11379–11448.

52 X. Ji, C. Held and G. Sadowski, *Fluid Phase Equilib.*, 2012, **335**, 64–73.

53 E. K. Karakatsani, L. G. Economou, M. C. Kroon, C. J. Peters and G. J. Witkamp, *J. Phys. Chem. C*, 2007, **111**, 15487–15492.

54 M. C. Kroon, E. K. Karakatsani, I. G. Economou, G. J. Witkamp and C. J. Peters, *J. Phys. Chem. B*, 2006, **110**, 9262–9269.

55 J. S. Andreu and L. F. Vega, *J. Phys. Chem. C*, 2007, **111**, 16028–16034.

56 J. S. Andreu and L. F. Vega, *J. Phys. Chem. B*, 2008, **112**, 15398–15406.

57 X. Y. Ji and H. Adidharma, *Fluid Phase Equilib.*, 2010, **293**, 141–150.

58 E. E. Alberto, L. L. Rossato, S. Hartz Alves, D. Alves and A. L. Braga, *Org. Biomol. Chem.*, 2011, **9**, 1001–1003.

59 C. Janiak, *J. Chem. Soc., Dalton Trans.*, 2000, 3885–3896.

60 H. A. Habib, A. Hoffmann, H. A. Höppe, G. Steinfeld and C. Janiak, *Inorg. Chem.*, 2009, **48**, 2166–2180; W. Zhang, X. Tang, H. Ma, W.-H. Sun and C. Janiak, *Eur. J. Inorg. Chem.*, 2008, 2830–2836; F. Neve and A. Crispini, *Cryst. Growth Des.*, 2001, **1**, 287–393.

61 K. M. Steed and J. W. Steed, *Chem. Rev.*, 2015, **115**, 2895–2933.

62 C. P. Brock, *Acta Crystallogr., Sect. B: Struct. Sci., Cryst. Eng. Mater.*, 2016, **72**, 807–821.

63 M. Enamullah, M. Ariful Islam and C. Janiak, *J. Mol. Struct.*, 2016, **1122**, 331–340.

64 V. Vasylyeva, T. Kedziorski, N. Metzler-Nolte, C. Schauerte and K. Merz, *Cryst. Growth Des.*, 2010, **10**, 4224–4226.

65 A. Gavezotti, *CrystEngComm*, 2008, **10**, 389–398.

66 M. Nishio, *Phys. Chem. Chem. Phys.*, 2011, **13**, 13873–13900; M. Nishio, Y. Umezawa, K. Honda, S. Tsuboyama and H. Suezawa, *CrystEngComm*, 2009, **11**, 1757–1788; M. Nishio, *CrystEngComm*, 2004, **6**, 130–158; C. Janiak, S. Temizdemir, S. Dechert, W. Deck, F. Girgsdies, J. Heinze,

M. J. Kolm, T. G. Scharmann and O. M. Zipffel, *Eur. J. Inorg. Chem.*, 2000, 1229–1241; Y. Umezawa, S. Tsuboyama, K. Honda, J. Uzawa and M. Nishio, *Bull. Chem. Soc. Jpn.*, 1998, **71**, 1207–1213; M. Nishio, M. Hirota and Y. Umezawa, *The CH/π interaction (evidence, nature and consequences)*, Wiley-VCH, New York, 1998.

67 D. H. Zaitsau, A. V. Yermalayeu, V. N. Emel'yanenko, S. Butler, T. Schubert and S. P. Verevkin, *J. Phys. Chem. B*, 2016, **120**, 7949–7957.

68 S. S. Y. Tan, D. R. MacFarlane, J. Upfal, L. A. Edye, W. O. S. Doherty, A. F. Patti, J. M. Pringle and J. L. Scott, *Green Chem.*, 2009, **11**, 339–345.

69 X. Han and D. W. Armstrong, *Org. Lett.*, 2005, **7**, 4205–4208.

70 S. P. Verevkin, D. H. Zaitsau, V. N. Emel'yanenko, A. V. Yermalayeu, C. Schick, H. Liu, E. J. Maginn, S. Bulut, I. Krossing and R. Kalb, *J. Phys. Chem. B*, 2013, **117**, 6473–6486.

71 D. H. Zaitsau, A. V. Yermalayeu, V. N. Emel'yanenko, S. P. Verevkin, U. Welz-Biermann and T. Schubert, *Science China Chemistry - Special Issue on "Ionic Liquids for Green Chemistry"*, 2012, **55**, 1525–1531.

72 D. H. Zaitsau, A. V. Yermalayeu, V. N. Emel'yanenko, S. P. Verevkin, U. Welz-Biermann and T. Schubert, *Science China Chemistry - Special Issue on "Ionic Liquids for Green Chemistry"*, 2012, **55**, 1525–1531.

73 J. S. Chickos, S. Hosseini, D. G. Hesse and J. F. Liebman, *Struct. Chem.*, 1993, **4**, 271–278.

74 J. M. Crosthwaite, M. J. Muldoon, J. K. Dixon, J. L. Anderson and J. F. Brennecke, *J. Chem. Thermodyn.*, 2005, **37**, 559–568.

75 D. H. Zaitsau, M. Kaliner, S. Lerch, T. Strassner, V. N. Emel'yanenko and S. P. Verevkin, *Z. Anorg. Allg. Chem.*, 2017, **643**, 114–119.

76 S. P. Verevkin, V. N. Emel'yanenko, V. Diky, C. D. Muzny, R. D. Chirico and M. Frenkel, *J. Phys. Chem. Ref. Data*, 2013, **42**, 033102.

77 M. G. Voronkov, V. A. Klyuchnikov, S. N. Kolabin, G. N. Shvets, P. I. Varushin, E. N. Deryagina, N. A. Korchevin and S. I. Tsvetnitskaya, *Dokl. Akad. Nauk SSSR, Phys. Chem.*, 1989, **307**, 650–653.

78 V. Majer, V. Svoboda and H. V. Kehiaian, *Enthalpies of Vaporization of Organic Compounds: A Critical Review and Data Compilation*, IUPAC Chemical Data Series No. 32, Blackwell Scientific Publications, Oxford, 1985.

79 C. M. Hansen, *Prog. Org. Coat.*, 2004, **51**, 77–84.

80 B. Yoo, W. Afzal and J. M. Prausnitz, *Ind. Eng. Chem. Res.*, 2012, **51**, 9913–9917.

81 D. R. Lide, in *CRC handbook of chemistry and physics: a ready-reference book of chemical and physical data*, ed. D. R. Lide, CRC Press, Boca Raton, Florida, 2009.

82 A. Kraynov and T. E. Müller, in *Concepts for the stabilization of metal nanoparticles in ionic liquids, from: Applications of ionic liquids in science and technology*, ed. S. Handy, InTech, Croatia, 2011, pp. 235–260.

83 E. Redel, R. Thomann and C. Janiak, *Inorg. Chem.*, 2008, **47**, 14–16.

84 (*a*) A. K. Tiwari, V. K. Verma, T. A. Jain and P. K. Bajpai, *Nanomater. Energy*, 2014, 160–166; (*b*) K. N. Sharma, H. Joshi, V. V. Singh, P. Singh and A. K. Singh, *Dalton Trans.*, 2013, **42**, 3908–3918; (*c*) V. V. Singh, G. K. Rao, A. Kumar and A. K. Singh, *Dalton Trans.*, 2012, **41**, 1142–1145.

85 (*a*) K. Klauke, I. Gruber, T.-O. Knedel, L. Schmolke, J. Barthel, H. Breitzke, G. Buntkowsky and C. Janiak, *Organometallics*, 2018, **37**, 298–308; (*b*) R. Rishu, B. Prashanth, D. Bawari, U. Mandal, V. Verma, A. R. Choudhury and S. Singh, *Dalton Trans.*, 2017, **46**, 6291–6302; (*c*) K. N. Sharma, H. Joshi, A. K. Sharma, O. Prakash and A. K. Singh, *Organometallics*, 2013, **32**, 2443–2451.

86 Ernst Ruska-Centre for Microscopy and Spectroscopy with Electrons FEI Tecnai G2 F20, Journal of large-scale research facilities, 2, A77, 2016.

87 *Apex2, data collection program for the CCD area-detector system, SAINT, data reduction and frame integration program for the CCD area-detector system, Bruker analytical X-ray*.

88 G. Sheldrick, *Program SADABS: Area-detector absorption correction*, University of Göttingen, Germany, 1996.

89 G. Sheldrick, *Acta Crystallogr., Sect. A: Found. Crystallogr.*, 2008, **64**, 112–122.

90 *DIAMOND 4.4.0 for Windows*, Crystal Impact Gbr, Bonn, Germany; http://www.crystalimpact.com/diamond.

91 S. P. Verevkin, D. H. Zaitsau, V. N. Emel'yanenko and A. Heintz, *J. Phys. Chem. B*, 2011, **115**, 12889–12895.

92 G. Sauerbrey, *Z. Phys.*, 1959, **155**, 206–222.